Tunneling current of the Coulomb-coupled quantum dots embedded in n–n junction*

Yan Wei-Xian(阎维贤)[a)†], Zhao Ya-Ping(赵亚平)[a)], Wen Yu-Bing(温玉兵)[a)], Li Xiu-Ping(李秀平)[a)], Xu Li-Ping(许丽萍)[b)], and Gong Jian-Ping(宫建平)[c)]

[a)] *College of Physics and Electronics, Shanxi University, Taiyuan* 030006, *China*
[b)] *Department of Physics, North University of China, Taiyuan* 030051, *China*
[c)] *Department of Physics, Jinzhong University, Yuci* 030600, *Shanxi Province, China*

(Received 27 April 2009; revised manuscript received 22 June 2009)

Taking account of the electron–electron (hole) and electron–hole interactions, the tunneling processes of the main quantum dot (QD) Coulomb-coupled with a second quantum dot embedded in n–n junction have been investigated. The eighteen resonance mechanisms involved in the tunneling processes of the system have been identified. It is found that the tunneling current depends sensitively on the electron occupation number in the second quantum dot. When the electron occupation number in the second dot is tiny, both the tunneling current peaks and the occupation number plateaus in the main QD are determined by the intra-resonance mechanism. The increase of the electron occupation number in the second dot makes the inter-resonance mechanism participate in the transport processes. The competition between the inter and intra resonance mechanisms persists until the electron occupation number in the second dot reaches around unity, leading to the consequence that the inter-resonance mechanisms completely dominate the tunneling processes.

Keywords: single-electron tunneling, exciton complexes, quantum dots

PACC: 7335C, 7135, 7320D

1. Introduction

Semiconductor quantum dot (QD) has become one of the indispensable members in the electro-optical devices such as light-emitting diodes, optical switches and quantum information processing unit.[1−8] A single QD can function as a microelectronic unit such as a transistor, forming the basis of nanoelectronics.[9] The fine energy structures of the resonant/bound state, such as exciton, charged exciton (trion), or even biexciton structure due to electron–hole correlations[10−26] have provided ways of controlling the electron and hole dynamics by using the optical light, paving road for the solid state realization of the quantum communication and quantum computing.[4,13,21−23,27−30] In the studies of these potential properties, many novel theoretical and experimental phenomena have been disclosed. Among these findings, strong photon antibunching[25−27] resulting from the optical processes involved in the fine structures due to the electron–hole exchange in QD, Coulomb blockade due to Hubbard interaction among the carriers,[31] virtual photon intermediated Förster transfer,[29] and Kondo effect in the QDs due to the coupling of local degenerate state to the mobile electron reservoirs,[32−39] are the typical examples. Exploration of all these phenomena and applications in semiconductor QD necessitates the studies on the resonance energy structures in the transport and optical processes of single-electron transistor (SET), consisting of the three-terminals: source, gate and drain. For example, the self-assembled direct-gap InAs/GaAs QD buried into the source and drain[9] is a prototypical SET.

Ediger and co-authors studied the photoluminescence of the close-symmetric InAs/GaAs and InGaAs/GaAs coupled QDs, where the fine structures of exciton complexes, singly-charged, the trion, doubly-charged and neutral excitons underline the peaks of the spectra.[17] In their investigations, the role of the resonance mechanisms played by the electron–hole correlations on the electronic transport properties of QDs has been emphasized.

In the framework of the Keldysh non-equilibrium Green's function, Kuo and Chang studied the SET,

*Project supported by the National Natural Science Foundation of China (Grant No. 60776062), the National Fundamental Fund of Personnel Training (Grant No. J0730317), and the Natural Science Foundation of Shanxi Province, China (Grant Nos. 2008011001-1 and 2008011001-2).

†Corresponding author. E-mail: yanwxsxu@yahoo.com.cn

© 2010 Chinese Physical Society and IOP Publishing Ltd

where a single QD is embedded in p–n, and n–n junctions.[10,40] It is found that the sharp peaks both in tunneling current and emission spectrum, reveal the exciton, charged exciton, and even biexciton mechanisms, coexisting in the complicated optical and transport processes. Their studies provide a precise method for measuring the exciton binding energy and electron–electron repulsion energy.[40] Inspired by their work, we introduce the second QD into the system. The second QD can be considered as an impurity dot or deliberately manufactured using Stranski–Krastanow method, through which controllable multi-dot system can be produced. The two QDs are coupled together through the Coulomb interactions.[14,17] Using the Keldysh formalism, we obtain a formidable closed set of equations, through which the effect of the Coulomb interactions among the charged carriers on the tunneling current has been found. All the resonance mechanisms involved in the tunneling processes due to the electron and hole correlations have been identified and analysed through the analytical and numerical methods. The influence of electron number in the second QD on the modification of the electronic transport has been given in details, the neutral and charged electron and hole complexes have been associated with the resonance mechanisms in the tunneling processes.

The rest of the paper is organized as follows: Section 2 gives the background, where the Hamiltonian governing the electron tunneling processes and some assumptions are proposed. The analytical expression of the tunneling current is derived in Section 3, where the influences of the bias and gate voltages with the different electron occupation number in the second QD on the tunneling processes in the main QD is discussed in detail. Section 4 gives a summary of our work.

2. The model and formalism

The single-electron tunneling device considered here consists of n-type source-drain junctions, the main QD and the n-type second side-dot, whose Hamiltonian can be separated into two parts, $\mathcal{H} = \mathcal{H}_0 + \mathcal{H}_{\rm coul}$. $\mathcal{H}_0$ describes the free electrons and holes part together with the hopping between the main QD and source-drain junctions, and can be written as follows:

$$\begin{aligned}\mathcal{H}_0 =& \sum_{i=({\rm e,h}),\sigma} E_i d^\dagger_{i,\sigma} d_{i,\sigma} + \sum_{\sigma} E_{2{\rm e}} d^\dagger_{2{\rm e},\sigma} d_{2{\rm e},\sigma} \\ &+ \sum_{k,\sigma,l={\rm L,R}} \epsilon_k c^\dagger_{k,\sigma,l} c_{k,\sigma,l} \\ &+ \sum_{k\sigma l} \left(V_{k,\sigma,l} c^\dagger_{k,\sigma,l} d_{{\rm e},\sigma} + V^\dagger_{k,\sigma,l} d^\dagger_{{\rm e},\sigma} c_{k,\sigma,l} \right), \quad (1)\end{aligned}$$

where $d_{i,\sigma}, (d^\dagger_{i,\sigma})$ represents the annihilation (creation) electron/hole operators with spin σ in the intrinsic main QD; $d_{2{\rm e}}, (d^\dagger_{2{\rm e}})$, the annihilation (creation) electron operator with spin σ in the n-type second side-QD; $c_{k,\sigma,l}, (c^\dagger_{k,\sigma,l})$, the annihilation (creation) electron operators in source and drain, and the last term describes the hopping between the source, drain and main intrinsic QD, the absence of hopping between the main QD and the second QD has been assumed.[14]

A laser light excites the carriers in the wetting layer, and this pumping process is described in a semi-classical way as,

$$\begin{aligned}\mathcal{H}_{\rm opex} =& \sum_{k\sigma l} \Big(\lambda_0 \, {\rm e}^{{\rm i}\omega_0 t} b_{{\rm e},k,\sigma} b_{{\rm h},k,-\sigma} \\ &+ \lambda_0^\dagger \, {\rm e}^{-{\rm i}\omega_0 t} b^\dagger_{{\rm h},k,-\sigma} b^\dagger_{{\rm e},k,\sigma} \Big),\end{aligned}$$

where $b_{{\rm e},k,\sigma}$ and $b_{{\rm h},k,-\sigma}$ are the paired electron–hole annihilation operators in the wetting layer. The optically-generated carriers in the wetting layer undergoes relaxation processes, such as electron–phonon and impurity scattering processes into the main QDs. The phonon absorption is neglected here due to the phonon-bottleneck effect in the low temperature situation.[41]

Rough estimate for the tunneling rate $\Gamma_{\rm e} (\equiv \Gamma_{\rm L} + \Gamma_{\rm R})$, ($\Gamma_{{\rm L}(R)}$ is the tunneling rate between the main QD and the left (right) lead) shows that it is much larger than the electrons capture rate $\gamma_{{\rm e},c}$ from wetting layer to the main QD. So the pumping-induced electron occupation number can be safely neglected. For the hole capture from the wetting layer to the main QD, the situation is just the opposite, the hole occupation number can be estimated semiclassically as[10]

$$n_{{\rm h},\sigma} = \frac{\gamma_{\rm h,c} N_{{\rm h},\boldsymbol{k}}}{\gamma_{\rm h,c} N_{{\rm h},-\boldsymbol{k}} + R_{\rm eh} N_{{\rm e}\sigma} + \Gamma_{{\rm h},s}}, \quad (2)$$

where $N_{{\rm h},\boldsymbol{k}} \equiv \langle b^\dagger_{{\rm h},\boldsymbol{k}} b_{{\rm h},\boldsymbol{k}} \rangle$, represents hole number in the wetting layer generated by the light excitation; $\gamma_{\rm h,c}$ is the capture rate from the wetting layer to the main QD; $R_{\rm eh}$ and $\Gamma_{{\rm h},s}$ are the phenomenological

electron–hole and nonradiative recombination rates respectively. $N_{\mathrm{e},\sigma}$ denotes the electron occupation number in the main QD due to tunneling, which can be determined self-consistently.

Since the tunneling rate Γ_{e} is much larger than the electron–hole recombination rate R_{eh}, during the time scale of interest, the holes are persistently present in the process of the electron tunneling. The electrons and holes Coulomb interactions $\mathcal{H}_{\mathrm{coul}}$ can be written as follows:

$$H_{\mathrm{coul}} = \sum_{i,\sigma}^{(\mathrm{e,2e,h})} U_{i,i} d^{\dagger}_{i,\sigma} d_{i,\sigma} d^{\dagger}_{i,-\sigma} d_{i,-\sigma} + \sum_{i\neq j,\sigma,\sigma'}^{(\mathrm{e,h})} U_{i,j} d^{\dagger}_{i,\sigma} d_{i,\sigma} d^{\dagger}_{j,\sigma'} d_{j,\sigma'} + \sum_{i,\sigma,\sigma'}^{(\mathrm{e,h})} U_{i,2\mathrm{e}} d^{\dagger}_{i,\sigma} d_{i,\sigma} d^{\dagger}_{2\mathrm{e},\sigma'} d_{2\mathrm{e},\sigma'}, \quad (3)$$

where the first term describes the electron–electron, hole–hole interactions in the main QD and electron–electron interaction in the second QD; the second term, describes the electron–hole interactions in the main QD, and the last term describes the electron–electron/hole interactions between the side QD and main QD. The above Coulomb coupling term $\mathcal{H}_{\mathrm{coul}}$ can be rewritten explicitly as,

$$H_{\mathrm{coul}} = \sum_{\sigma=\uparrow,\downarrow} \Big[U_{\mathrm{e}} \hat{N}_{\mathrm{e},\sigma} \hat{N}_{\mathrm{e},-\sigma} - U_{\mathrm{eh}} \left(\hat{N}_{\mathrm{e},\sigma} \hat{n}_{\mathrm{h},\sigma} + \hat{N}_{\mathrm{e},\sigma} \hat{n}_{\mathrm{h},-\sigma} \right) + U_{\mathrm{h}} \hat{n}_{\mathrm{h},\sigma} \hat{n}_{\mathrm{h},-\sigma} + U_{2\mathrm{e}} (\hat{n}_{2\mathrm{e},\sigma} \hat{n}_{2\mathrm{e},-\sigma}) + U_{ey} \left(\hat{n}_{\mathrm{e},\sigma} \hat{n}_{2\mathrm{e},\sigma} + \hat{N}_{\mathrm{e},\sigma} \hat{n}_{2\mathrm{e},-\sigma} \right) - U_{\mathrm{h}y} \left(\hat{n}_{\mathrm{h},\sigma} \hat{n}_{2\mathrm{e},\sigma} + \hat{n}_{\mathrm{h},\sigma} \hat{n}_{2\mathrm{e},-\sigma} \right) \Big], \quad (4)$$

where $U_{\mathrm{e}}, U_{\mathrm{eh}}, U_{\mathrm{h}}$ are the electron–electron, electron–hole and hole–hole intra-interaction strengths in the main QD respectively, while $U_{2\mathrm{e}}$ is the electron–electron interaction strengths in the second QD, U_{ey} and $U_{\mathrm{h}y}$ are the interaction strengths between the electrons in the second QD and electrons and holes in the main QD respectively.

In the following section, the closed form of solutions for the tunneling current will be obtained in the framework of the Keldysh formalism.

3. The tunneling current

The tunneling rate $\Gamma_{\mathrm{L,R}}$ between the source/drain and main QD is much larger than both the capture rate of the electron γ_{ec}, and the electron–hole recombination rate R_{eh}; the capture rate of the electron is determined by the electron–phonon and electron–impurity scattering mechanisms. This assumption indicates that electron relaxation from the wetting layer to the main QD has been neglected in the time scale of interest.[10] The stationary tunneling current flowing through the main QD can be calculated as follows:[10,42,43]

$$J = -\frac{2e}{h} \int \frac{\mathrm{d}\epsilon}{2\pi} \frac{\Gamma_{\mathrm{L}}(\epsilon)\Gamma_{\mathrm{R}}(\epsilon)}{\Gamma_{\mathrm{L}}(\epsilon) + \Gamma_{\mathrm{R}}(\epsilon)} \times \left[f_{\mathrm{L}}(\epsilon - \mu_{\mathrm{L}}) - f_{\mathrm{R}}(\epsilon - \mu_{\mathrm{R}}) \right] \mathcal{A}_{\sigma}(\epsilon), \quad (5)$$

where $\mathcal{A}_{\sigma}(\epsilon)$ is the spectral function, and can be determined from the imaginary part of the retarded Green's function $G^{\mathrm{r}}_{\mathrm{e},\sigma}(\epsilon)$. It is worth while noting that the spectral function $\mathcal{A}_{\sigma}(\epsilon)$ here is determined by the electron–electron as well as electron–hole interactions. The chemical potential difference from left and right electrodes defines the bias between the two electrodes: $\mu_{\mathrm{L}} - \mu_{\mathrm{R}} = eV_a$, as the usual way. In order to calculate the tunneling current, the central task is to calculate the following retarded Green's function,

$$G^{\mathrm{r}}_{\mathrm{e},\sigma}(t) = -\mathrm{i}\theta(t) \left\langle \left\{ d_{\mathrm{e},\sigma}(t), d^{\dagger}_{\mathrm{e},\sigma}(0) \right\} \right\rangle, \quad (6)$$

where $\theta(t)$ is the Heavside step function. The equation of motion for the retarded Green's function can be obtained by using the Heisenberg equation of motion for the fermion operators. After the Fourier transformation, $G^{\mathrm{r}}_{\mathrm{e}\sigma}(\epsilon)$ can be evaluated to be

$$\left(\epsilon - E_{\mathrm{e}} + \mathrm{i}\frac{\Gamma_{\mathrm{e}}}{2} \right) G^{\mathrm{r}}_{\mathrm{e},\sigma}(\epsilon) = 1 + U_{\mathrm{e}} G^{\mathrm{r}}_{\mathrm{ee},\sigma}(\epsilon) - U_{\mathrm{eh}} \left[G^{\mathrm{r}}_{\mathrm{eh},1}(\epsilon) + G^{\mathrm{r}}_{\mathrm{eh},2}(\epsilon) \right] + U_{ey} \left[G^{\mathrm{r}}_{ey,1}(\epsilon) + G^{\mathrm{r}}_{ey,2}(\epsilon) \right], \quad (7)$$

where E_{e} is the electron ground state energy level in the main QD, $\Gamma_{\mathrm{e}}(\epsilon) \equiv \Gamma_{\mathrm{L}}(\epsilon) + \Gamma_{\mathrm{R}}(\epsilon)$; the lowest order coupling between the electrodes and the main QD has been adopted.[10]

From the above equation, the calculation of the single-particle Green's function necessitates the evaluation of the two-particle retarded Green's functions $G^{\rm r}_{{\rm ee},\sigma}(t)$, $G^{\rm r}_{{\rm eh}1}(t)$, $G^{\rm r}_{{\rm eh}2}(t)$, $G^{\rm r}_{{\rm e}y1}(t)$, and $G^{\rm r}_{{\rm e}y2}(t)$, which are defined as

$$G^{\rm r}_{{\rm ee},\sigma}(t) = -\,{\rm i}\theta(t)\left\langle\{d_{{\rm e},\sigma}(t)\hat{N}_{{\rm e},-\sigma}(t), d^{\dagger}_{{\rm e},\sigma}(0)\}\right\rangle, \tag{8a}$$

$$G^{\rm r}_{{\rm eh}1}(t) = -\,{\rm i}\theta(t)\left\langle\{d_{{\rm e},\sigma}(t)\,\hat{n}_{{\rm h},\sigma}(t), d^{\dagger}_{{\rm e},\sigma}(0)\}\right\rangle, \tag{8b}$$

$$G^{\rm r}_{{\rm eh}2}(t) = -\,{\rm i}\theta(t)\left\langle\{d_{{\rm e},\sigma}(t)\hat{n}_{{\rm h},-\sigma}(t), d^{\dagger}_{{\rm e},\sigma}(0)\}\right\rangle, \tag{8c}$$

$$G^{\rm r}_{{\rm e}y1}(t) = -\,{\rm i}\theta(t)\left\langle\{d_{{\rm e},\sigma}(t)\,\hat{n}_{2{\rm e},\sigma}(t), d^{\dagger}_{{\rm e},\sigma}(0)\}\right\rangle, \tag{8d}$$

$$G^{\rm r}_{{\rm e}y2}(t) = -\,{\rm i}\theta(t)\left\langle\{d_{{\rm e},\sigma}(t)\,\hat{n}_{2{\rm e},-\sigma}(t), d^{\dagger}_{{\rm e},\sigma}(0)\}\right\rangle. \tag{8e}$$

The Fourier transform of the above two-particle retarded Green's function can be obtained as follows:

$$\left(\epsilon - E_{\rm e} - U_{\rm e} + {\rm i}\frac{\Gamma_{\rm e}}{2}\right) G^{\rm r}_{{\rm ee},\sigma}(\epsilon) = N_{{\rm e},-\sigma} - U_{\rm eh}[G^{\rm r}_{{\rm ehe},1}(\epsilon) + G^{\rm r}_{{\rm ehe},2}(\epsilon)] + U_{{\rm e}y}[G^{\rm r}_{{\rm e}y{\rm e},1}(\epsilon) + G^{\rm r}_{{\rm e}y{\rm e},2}(\epsilon)], \tag{9a}$$

$$\left(\epsilon - E_{\rm e} + U_{\rm eh} + {\rm i}\frac{\Gamma_{\rm e}}{2}\right) G^{\rm r}_{{\rm eh}1}(\epsilon) = n_{{\rm h},\sigma} + U_{\rm e}G^{\rm r}_{{\rm ehe},1}(\epsilon) - U_{\rm eh}G^{\rm r}_{\rm ehh}(\epsilon) + U_{{\rm e}y}[G^{\rm r}_{{\rm eh}y1}(\epsilon) + G^{\rm r}_{{\rm eh}y2}(\epsilon)], \tag{9b}$$

$$\left(\epsilon - E_{\rm e} + U_{\rm eh} + {\rm i}\frac{\Gamma_{\rm e}}{2}\right) G^{\rm r}_{{\rm eh}2}(\epsilon) = n_{{\rm h},-\sigma} + U_{\rm e}G^{\rm r}_{{\rm ehe}2}(\epsilon) - U_{\rm eh}G^{\rm r}_{\rm ehh}(\epsilon) + U_{{\rm e}y}[G^{\rm r}_{{\rm eh}'y1}(\epsilon) + G^{\rm r}_{{\rm eh}'y2}(\epsilon)], \tag{9c}$$

$$\left(\epsilon - E_{\rm e} - U_{{\rm e}y} + {\rm i}\frac{\Gamma_{\rm e}}{2}\right) G^{\rm r}_{{\rm e}y1}(\epsilon) = n_{2{\rm e}\sigma} + U_{\rm e}G^{\rm r}_{{\rm e}y{\rm e},1}(\epsilon) + U_{{\rm e}y}G^{\rm r}_{{\rm e}yy}(\epsilon) - U_{\rm eh}[G^{\rm r}_{{\rm eh}y1}(\epsilon) + G^{\rm r}_{{\rm eh}'y1}(\epsilon)], \tag{9d}$$

$$\left(\epsilon - E_{\rm e} - U_{{\rm e}y} + {\rm i}\frac{\Gamma_{\rm e}}{2}\right) G^{\rm r}_{{\rm e}y2}(\epsilon) = n_{2{\rm e},-\sigma} + U_{\rm e}G^{\rm r}_{{\rm e}y{\rm e},2}(\epsilon) + U_{{\rm e}y}G^{\rm r}_{{\rm e}yy}(\epsilon) - U_{\rm eh}[G^{\rm r}_{{\rm eh}y2}(\epsilon) + G^{\rm r}_{{\rm eh}'y2}(\epsilon)]. \tag{9e}$$

The determination of the two-particle Green's function requires the solutions of the three-particle retarded Green's function, which consist of the following 10 retarded Green's functions:

$$G^{\rm r}_{\rm ehe1}(t) = -{\rm i}\theta(t)\left\langle\left\{\hat{N}_{{\rm e},-\sigma}(t)\,\hat{n}_{{\rm h},\sigma}(t)\,d_{{\rm e},\sigma}(t), d^{\dagger}_{{\rm e},\sigma}(0)\right\}\right\rangle, \tag{10a}$$

$$G^{\rm r}_{\rm ehe2}(t) = -{\rm i}\theta(t)\left\langle\left\{\hat{N}_{{\rm e},-\sigma}(t)\,\hat{n}_{{\rm h},-\sigma}(t)\,d_{{\rm e},\sigma}(t), d^{\dagger}_{{\rm e},\sigma}(0)\right\}\right\rangle, \tag{10b}$$

$$G^{\rm r}_{\rm ehh}(t) = -{\rm i}\theta(t)\left\langle\left\{\hat{n}_{{\rm h},\sigma}\hat{n}_{{\rm h},-\sigma}(t)\,d_{{\rm e},\sigma}(t), d^{\dagger}_{{\rm e},\sigma}(0)\right\}\right\rangle, \tag{10c}$$

$$G^{\rm r}_{{\rm e}y{\rm e}1}(t) = -{\rm i}\theta(t)\left\langle\left\{\hat{N}_{{\rm e},-\sigma}(t)\,\hat{n}_{2{\rm e},\sigma}(t)\,d_{{\rm e},\sigma}(t), d^{\dagger}_{{\rm e},\sigma}(0)\right\}\right\rangle, \tag{10d}$$

$$G^{\rm r}_{{\rm e}y{\rm e}2}(t) = -{\rm i}\theta(t)\left\langle\left\{\hat{N}_{{\rm e},-\sigma}(t)\,\hat{n}_{2{\rm e},-\sigma}(t)\,d_{{\rm e},\sigma}(t), d^{\dagger}_{{\rm e},\sigma}(0)\right\}\right\rangle, \tag{10e}$$

$$G^{\rm r}_{{\rm e}yy}(t) = -{\rm i}\theta(t)\left\langle\left\{\hat{n}_{2{\rm e},\sigma}(t)\,\hat{n}_{2{\rm e},-\sigma}(t)\,d_{{\rm e},\sigma}(t), d^{\dagger}_{{\rm e},\sigma}(0)\right\}\right\rangle, \tag{10f}$$

$$G^{\rm r}_{{\rm eh}y1}(t) = -{\rm i}\theta(t)\left\langle\left\{\hat{n}_{{\rm h},\sigma}(t)\,\hat{n}_{2{\rm e},\sigma}(t)\,d_{{\rm e},\sigma}(t), d^{\dagger}_{{\rm e},\sigma}(0)\right\}\right\rangle, \tag{10g}$$

$$G^{\rm r}_{{\rm eh}y2}(t) = -{\rm i}\theta(t)\left\langle\left\{\hat{n}_{{\rm h},\sigma}(t)\,\hat{n}_{2{\rm e},-\sigma}(t)\,d_{{\rm e},\sigma}(t), d^{\dagger}_{{\rm e},\sigma}(0)\right\}\right\rangle, \tag{10h}$$

$$G^{\rm r}_{{\rm e}\bar{\rm h}y1}(t) = -{\rm i}\theta(t)\left\langle\left\{\hat{n}_{{\rm h},-\sigma}(t)\,\hat{n}_{2{\rm e},\sigma}(t)\,d_{{\rm e},\sigma}(t), d^{\dagger}_{{\rm e},\sigma}(0)\right\}\right\rangle, \tag{10i}$$

$$G^{\rm r}_{{\rm e}\bar{\rm h}y2}(t) = -{\rm i}\theta(t)\left\langle\left\{\hat{n}_{{\rm h},-\sigma}(t)\,\hat{n}_{2{\rm e},-\sigma}(t)\,d_{{\rm e},\sigma}(t), d^{\dagger}_{{\rm e},\sigma}(0)\right\}\right\rangle. \tag{10j}$$

The hierarchy of the equations of motion of the retarded Green's function beyond the three-particles retarded Green's function will continue till the six-particle retarded Green's function, where the hierarchy terminates. The last but only six-particle retarded Green's function $G^{\rm r}_{{\rm ehh}y{\rm e}}(t)$ is defined as follows:

$$G^{\rm r}_{{\rm ehh}y{\rm e}}(t) = -{\rm i}\theta(t)\left\langle\{d_{{\rm e},\sigma}(t)\hat{N}_{{\rm e},-\sigma}(t)\hat{n}_{{\rm h},\sigma}(t)\hat{n}_{{\rm h},-\sigma}(t)\hat{n}_{2{\rm e},\sigma}(t)\hat{n}_{2{\rm e},-\sigma}(t), d^{\dagger}_{{\rm e},\sigma}(0)\}\right\rangle. \tag{11}$$

This six-particle retarded Green's function obeys the following equation of motion

$${\rm i}\hbar\frac{\partial}{\partial t}G^{\rm r}_{{\rm ehh}y{\rm e}}(t) = \delta(t)\,N_{{\rm e},-\sigma}n_{{\rm h},\sigma}n_{{\rm h},-\sigma}n_{2{\rm e},\sigma}n_{2{\rm e},-\sigma} + E_{\rm e}G^{\rm r}_{{\rm ehh}y{\rm e}}(t) - {\rm i}\frac{\Gamma_{\rm e}}{2}G^{\rm r}_{{\rm ehh}y{\rm e}}(t)$$

$$+ U_{\rm e} G^{\rm r}_{\rm ehhyye}(t) - 2U_{\rm eh} G^{\rm r}_{\rm ehhyye}(t) + 2U_{ey} G^{\rm r}_{\rm ehhyye}(t). \tag{12}$$

Fourier transform of the above six-particle retarded Green's function $G^{\rm r}_{\rm ehhyye}(t)$ leads to the following expression,

$$G^{\rm r}_{\rm ehhyye}(\epsilon) = \frac{N_{\rm e,-\sigma} n_{\rm h,\sigma} n_{\rm h,-\sigma} n_{\rm 2e,\sigma} n_{\rm 2e,-\sigma}}{\epsilon - E_{\rm e} - U_{\rm e} - 2U_{ey} + 2U_{\rm eh} + {\rm i}\Gamma_{\rm e}/2}. \tag{13}$$

For saving space, the definition and equations of motion of the four-particle retarded Green's function and beyond are left out. The final result for the single-particle retarded Green's function $G^{\rm r}_{\rm e,\sigma}(\epsilon)$ can be obtained as:

$$G^{\rm r}_{\rm e,\sigma}(\epsilon) = (1 - N_{\rm e,-\sigma})\mathcal{F}_1(\epsilon) + N_{\rm e,-\sigma}\mathcal{F}_2(\epsilon), \tag{14}$$

where $\mathcal{F}_1(\epsilon)$ and $\mathcal{F}_2(\epsilon)$ are defined as follows:

$$\begin{aligned}\mathcal{F}_1(\epsilon) \equiv \Bigg(& \frac{(1 - \mathcal{N}_{\rm h,\sigma} + \mathcal{S}_{\rm h,\sigma})(1 - \mathcal{N}_{\rm 2e,\sigma} + \mathcal{S}_{\rm 2e,\sigma})}{\epsilon - E_{\rm e} + {\rm i}\Gamma_{\rm e}/2} + \frac{(\mathcal{N}_{\rm h,\sigma} - 2\mathcal{S}_{\rm h,\sigma})(1 - \mathcal{N}_{\rm 2e,\sigma} + \mathcal{S}_{\rm 2e,\sigma})}{\epsilon - E_{\rm e} + U_{\rm eh} + {\rm i}\Gamma_{\rm e}/2} \\ & + \frac{(1 - \mathcal{N}_{\rm h,\sigma} + \mathcal{S}_{\rm h,\sigma})(\mathcal{N}_{\rm 2e,\sigma} - 2\mathcal{S}_{\rm 2e,\sigma})}{\epsilon - E_{\rm e} - U_{ey} + {\rm i}\Gamma_{\rm e}/2} + \frac{\mathcal{S}_{\rm h,\sigma}(1 - \mathcal{N}_{\rm 2e,\sigma} + \mathcal{S}_{\rm 2e,\sigma})}{\epsilon - E_{\rm e} + 2U_{\rm eh} + {\rm i}\Gamma_{\rm e}/2} + \frac{\mathcal{S}_{\rm 2e,\sigma}(1 - \mathcal{N}_{\rm h,\sigma} + \mathcal{S}_{\rm h,\sigma})}{\epsilon - E_{\rm e} - 2U_{ey} + {\rm i}\Gamma_{\rm e}/2} \\ & + \frac{(\mathcal{N}_{\rm h,\sigma} - 2\mathcal{S}_{\rm h,\sigma})(\mathcal{N}_{\rm 2e,\sigma} - 2\mathcal{S}_{\rm 2e,\sigma})}{\epsilon - E_{\rm e} - U_{ey} + U_{\rm eh} + {\rm i}\Gamma_{\rm e}/2} + \frac{\mathcal{S}_{\rm h,\sigma}(\mathcal{N}_{\rm 2e,\sigma} - 2\mathcal{S}_{\rm 2e,\sigma})}{\epsilon - E_{\rm e} - U_{ey} + 2U_{\rm eh} + {\rm i}\Gamma_{\rm e}/2} \\ & + \frac{\mathcal{S}_{\rm 2e,\sigma}(\mathcal{N}_{\rm h\sigma} - 2\mathcal{S}_{\rm h,\sigma})}{\epsilon - E_{\rm e} - 2U_{ey} + U_{\rm eh} + {\rm i}\Gamma_{\rm e}/2} + \frac{\mathcal{S}_{\rm 2e,\sigma}\mathcal{S}_{\rm h,\sigma}}{\epsilon - E_{\rm e} - 2U_{ey} + 2U_{\rm eh} + {\rm i}\Gamma_{\rm e}/2}\Bigg), \end{aligned} \tag{15}$$

and

$$\begin{aligned}\mathcal{F}_2(\epsilon) \equiv \Bigg(& \frac{(1 - \mathcal{N}_{\rm h,\sigma} + \mathcal{S}_{\rm h,\sigma})(1 - \mathcal{N}_{\rm 2e,\sigma} + \mathcal{S}_{\rm 2e,\sigma})}{\epsilon - E_{\rm e} - U_{\rm e} + {\rm i}\Gamma_{\rm e}/2} + \frac{(\mathcal{N}_{\rm h,\sigma} - 2\mathcal{S}_{\rm h,\sigma})(1 - \mathcal{N}_{\rm 2e,\sigma} + \mathcal{S}_{\rm 2e,\sigma})}{\epsilon - E_{\rm e} - U_{\rm e} + U_{\rm eh} + {\rm i}\Gamma_{\rm e}/2} \\ & \times \frac{(1 - \mathcal{N}_{\rm h,\sigma} + \mathcal{S}_{\rm h,\sigma})(\mathcal{N}_{\rm 2e,\sigma} - 2\mathcal{S}_{\rm 2e,\sigma})}{\epsilon - E_{\rm e} - U_{\rm e} - U_{ey} + {\rm i}\Gamma_{\rm e}/2} + \frac{\mathcal{S}_{\rm h,\sigma}(1 - \mathcal{N}_{\rm 2e,\sigma} + \mathcal{S}_{\rm 2e,\sigma})}{\epsilon - E_{\rm e} - U_{\rm e} + 2U_{\rm eh} + {\rm i}\Gamma_{\rm e}/2} + \frac{\mathcal{S}_{\rm 2e,\sigma}(1 - \mathcal{N}_{\rm h,\sigma} + \mathcal{S}_{\rm h,\sigma})}{\epsilon - E_{\rm e} - U_{\rm e} - 2U_{ey} + {\rm i}\Gamma_{\rm e}/2} \\ & + \frac{(\mathcal{N}_{\rm h,\sigma} - 2\mathcal{S}_{\rm h,\sigma})(\mathcal{N}_{\rm 2e,\sigma} - 2\mathcal{S}_{\rm 2e,\sigma})}{\epsilon - E_{\rm e} - U_{\rm e} - U_{ey} + U_{\rm eh} + {\rm i}\Gamma_{\rm e}/2} + \frac{\mathcal{S}_{\rm h,\sigma}(\mathcal{N}_{\rm 2e,\sigma} - 2\mathcal{S}_{\rm 2e,\sigma})}{\epsilon - E_{\rm e} - U_{\rm e} - U_{ey} + 2U_{\rm eh} + {\rm i}\Gamma_{\rm e}/2} \\ & + \frac{\mathcal{S}_{\rm 2e,\sigma}(\mathcal{N}_{\rm h,\sigma} - 2\mathcal{S}_{\rm h,\sigma})}{\epsilon - E_{\rm e} - U_{\rm e} - 2U_{ey} + U_{\rm eh} + {\rm i}\Gamma_{\rm e}/2} + \frac{\mathcal{S}_{\rm 2e,\sigma}\mathcal{S}_{\rm h,\sigma}}{\epsilon - E_{\rm e} - U_{\rm e} - 2U_{ey} + 2U_{\rm eh} + {\rm i}\Gamma_{\rm e}/2}\Bigg) \end{aligned} \tag{16}$$

with $\mathcal{N}_{\rm h,\sigma} = n_{\rm h,\sigma} + n_{\rm h,-\sigma}$, $\mathcal{N}_{\rm 2e,\sigma} = n_{\rm 2e,\sigma} + n_{\rm 2e,-\sigma}$, $\mathcal{S}_{\rm h,\sigma} = n_{\rm h,\sigma} n_{\rm h,-\sigma}$, $\mathcal{S}_{\rm 2e,\sigma} = n_{\rm 2e,\sigma} n_{\rm 2e,-\sigma}$.

Inspection of Eqs. (14)–(16) makes it clear that the electrons in the second QD participate the evolution of the retarded Green's function $G^{\rm r}_{\rm e,\sigma}(\epsilon)$ through the two approaches. Besides modifying the resonance energy structures (see below for detailed analysis) in the denominators, they also make the corresponding probabilities of these resonance mechanisms change substantially. The retarded Green's function in Eqs. (14)–(16) looks very cumbersome, however subsequent detailed analysis shows that the resonance structures can be classified into two main categories.

One category is intra-dot interactions induced resonance structures, which include intra-single electron $e_{\rm intra}$, ($\epsilon = E_{\rm e}$); intra-exciton $X_{\rm intra}$, ($\epsilon = E_{\rm e} - U_{\rm eh}$); intra-positive trion $X^{+}_{\rm intra}$, ($\epsilon = E_{\rm e} - 2U_{\rm eh}$); intra-2-electron $q^{2-}_{\rm intra}$, ($\epsilon = E_{\rm e} + U_{\rm e}$); intra-negative trion $X^{(-)}_{\rm intra}$, ($\epsilon = E_{\rm e} + U_{\rm e} - U_{\rm eh}$); and the intra-biexciton $[X^2]_{\rm intra}$, ($\epsilon = E_{\rm e} + U_{\rm e} - 2U_{\rm eh}$). Compared to the single QD case in Ref. [10], all these six terms have already been present in the single-QD case, but the probabilities for these resonance structures are altered remarkably in the presence of the Coulomb interaction between the two QDs. As far as the resonance structures are concerned, the newly developed twelve terms belong to the other catergory which are listed as follows (the subscript inter is used to denote the resonance mechanisms involving the interdot Coulomb interactions): the double electron $q^{2-}_{\rm inter}$, $\epsilon = E_{\rm e} + U_{ey}$; the first kind triple-electron $q^{3-}_{\rm 1,inter}$, $\epsilon = E_{\rm e} + 2U_{ey}$; the second kind triple-electron $q^{3-}_{\rm 2,inter}$, $\epsilon = E_{\rm e} + U_{\rm e} + U_{ey}$; the quadruple-electron $q^{4-}_{\rm inter}$ $E_{\rm e} + U_{\rm e} + 2U_{ey}$; the negative-trion $X^{-}_{\rm inter}$, $\epsilon = E_{\rm e} + U_{ey} - U_{\rm eh}$; the biexciton $[X^2]_{\rm inter}$,

$\epsilon = E_{\rm e} + U_{ey} - 2U_{\rm eh}$; the first kind double extra electrons attached exciton (3e + h quartet complexes) $X^{(2-)}_{1,\rm inter}$, $\epsilon = E_{\rm e} + U_{\rm e} + U_{ey} - U_{\rm eh}$; the second kind double extra electrons attached exciton (3e+h quartet complexes) $X^{(2-)}_{2,\rm inter}$, $\epsilon = E_{\rm e} + 2U_{ey} - U_{\rm eh}$; the first kind single extra electron attached biexciton (3e+2h quintet complexes) $[X^2]^{(-)}_{1,\rm inter}$, $\epsilon = E_{\rm e} + 2U_{ey} - 2U_{\rm eh}$; the second kind single extra electron attached biexciton (3e+2h quintet) $[X^2]^{(-)}_{2,\rm inter}$, $\epsilon = E_{\rm e} + U_{\rm e} + U_{ey} - 2U_{\rm eh}$; the triple extra electrons attached exciton (4e+h quintet) $X^{(3-)}_{\rm inter}$, $\epsilon = E_{\rm e} + U_{\rm e} + 2U_{ey} - U_{\rm eh}$; the double extra electrons attached biexciton (4e+2h sextet) $[X^2]^{(2-)}_{\rm inter}$, $\epsilon = E_{\rm e} + U_{\rm e} + 2U_{ey} - 2U_{\rm eh}$. The roles of all these resonance terms in the denominator together with the corresponding probabilities in the numerator played in the tunneling current have been analysed and discussed in detail in the following.

In order to give a quantitative picture of how the occupation number $n_{2{\rm e},\sigma}(\sigma =\uparrow,\downarrow)$, in the second QD influences the tunneling current, we give the detailed numerical analysis in the following. In the numerical simulation, we use the following parameters for the main QDs,[10] the electron and hole energy levels in the main QD in the absence of the biased voltage are $E_{\rm e} = -140$ meV, $E_{\rm h} = -125$ meV respectively, the Fermi level in the electrodes is chosen to be 70 meV below the electron energy level in the main QD, and is assumed to be 60.0 meV above the conduction band minimum, i.e., $E_{\rm F} = 60.0$ meV. The electron–electron, hole–hole, and electron–hole Coulomb interaction strengths are estimated to be $U_{\rm e} = 16.1$ meV, $U_{\rm h} = 18.5$ meV and $U_{\rm eh} = 16.7$ meV. The tunneling rates from both the left and the right leads have been taken to be equal, $\Gamma_{\rm L} = \Gamma_{\rm R}$, In the presence of both the gate voltage $V_{\rm g}$ and biased voltage $V_{\rm a}$, the energy levels for electron and hole in the main QD change according to the following rule, $E_{\rm e} + \alpha eV_{\rm a} - \beta eV_{\rm g}$, $E_{\rm h} + \alpha eV_{\rm a} - \beta eV_{\rm g}$ with $\alpha = 0.5$ and $\beta = 0.7$. In order to obtain the tunneling current in Eq. (5), the electron occupation number $N_{{\rm e},\sigma}$ due to tunneling in the main QD should be determined self-consistently through the following equation

$$N_{{\rm e},\sigma} = -\int \frac{{\rm d}\epsilon}{\pi} \frac{\Gamma_{\rm L}(\epsilon) f_{\rm L}(\epsilon) + \Gamma_{\rm R}(\epsilon) f_{\rm R}(\epsilon)}{\Gamma_{\rm L}(\epsilon) + \Gamma_{\rm R}(\epsilon)} \mathcal{A}_\sigma(\epsilon). \quad (17)$$

Without loss of generality, it is assumed that the hole number in the wetting layer generated by the light excitation $N_{{\rm h},\boldsymbol{k}}$ is linearly proportional to the light excitation power for low pumping intensity, which is characterized through a dimensionless quantity $\mathcal{I} \equiv \gamma_{{\rm h},c} N_{{\rm h},\boldsymbol{k}}/\Gamma_{{\rm h},s}$. In the following numerical simulation, $\Gamma_{{\rm h}s} = 0.20$ meV, $R_{\rm eh} = 10.0$ μeV, $\mathcal{I} = 0.90$. It is tacitly assumed that tunneling rate $\Gamma_{\rm L} = \Gamma_{\rm R} = 0.5$ in the following numerical presentation, unless we mention explicitly. The electron–electron and electron–hole Coulomb interaction strengths among the charged carriers between the two QDs are taken to be 14 meV and 12 meV respectively.

Figure 1 illustrates the electron occupation number in the main QD as a function of the gate voltage $eV_{\rm g}$, when the electron occupation number in the second QD takes the values 0.1, 0.5, 0.7, and 1.0 respectively. The plateaus correspond to the particular resonance mechanisms described above. When the electron occupation number in the second QD is small, say, $n_{2{\rm e},\sigma} = 0.1$, the eminent plateaus are similar to the case of the single QD,[10] but closer inspection of the curves indicates that there exist tiny shoulders between the main plateaus. This phenomenon becomes more pronounced in the tunneling current, as shown in Fig. 2, where the occupation number in the second QD is gradually increased from 0.1 to the maximum value of unity in steps 0.1. From Fig. 2, it can be clearly seen that when the electron occupation number is small (see Fig. 2(a)), the peaks appear in the same positions as in the case for a single QD, except that two additional peaks appear at $eV_{\rm g} = 119.6$ meV and 143 meV, and a number of shoulders emerge as satellites around some of these sharp peaks. The satellite peak at $eV_{\rm g} = 119.6$ meV is attributed to two possible mechanisms: $q^{2-}_{\rm inter}$, and $X^{(2-)}_{1,\rm inter}$, whose resonance energies are almost identical.

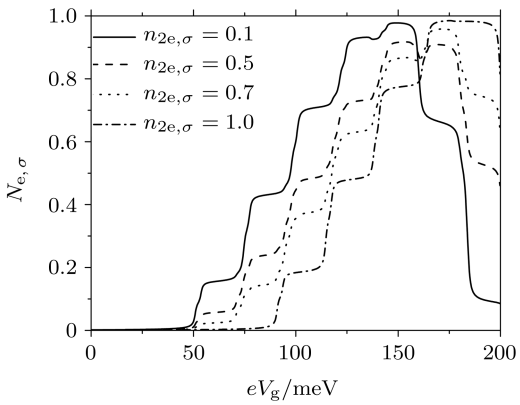


Fig. 1. The occupation number of the electrons $N_{{\rm e},\sigma}$ in the main quantum dot versus the gate voltage potential $eV_{\rm g}$ for different values of the electron occupation number in the second QD at zero temperature: $n_{2{\rm e},\sigma} = 0.1$ (solid), 0.5 (dashed), 0.7 (dotted) and 1.0 (dot-dashed).

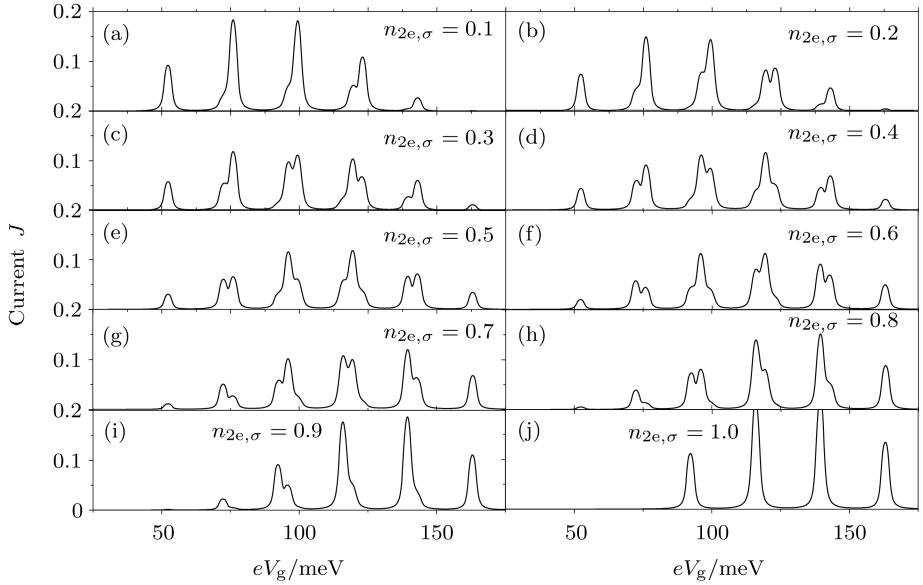


Fig. 2. The tunneling current J in the main QD versus the gate voltage potential eV_g for different values of occupation number of electrons in the second QD at zero temperature: the value of the occupation number of electrons in the second QD changes from 0.1 to maximum 1.0 in steps of 0.1 from Fig. 2(a) to Fig. 2(j), showing the detailed variation of the tunneling current.

While the other peak at $eV_g = 143$ meV results from the first-kind inter-triple electron mechanism $q^{3-}_{\rm inter}$. The number of peaks in the tunneling current has a tendency to increase and reaches maximum when the occupation number in the second QD is close to 0.5. Beyond 0.5, the number of the peaks begins to decrease, and only four sharp peaks survive when $n_{2e,\sigma}$ reaches unity. Let us focus on the two subpanels, where $n_{2e,\sigma} = 0.5, 1.0$ respectively. In the former subpanel (Fig. 2(e)), 10 peaks as well as additional two shoulders emerge, and these peaks and shoulders match in sequence the following resonance mechanisms from lower to higher energies: $X^{+}_{\rm intra}$, ($\approx$ 52.2 meV); $[X^2]_{\rm inter}$, ($\approx$ 72.4 meV); $[X]_{\rm intra}$, ($\approx$ 76 meV); $[X^2]^{(-)}_{\rm inter}$, ($\approx$ 91.4 meV); $X^{-}_{\rm inter}$, ($\approx$ 96 meV); $X^{-}_{\rm intra}$, ($\approx$ 99.2 meV); $X^{(2-)}_{2,\rm inter}$, ($\approx$ 116 meV); $X^{(2-)}_{1,\rm inter}$ (and $q^{2-}_{\rm inter}$), ($\approx$ 119.4 meV); $q^{2-}_{\rm intra}$, ($\approx$ 123.7 meV); $q^{3-}_{1,\rm inter}$ (and $X^{(3-)}_{\rm inter}$), ($\approx$ 139.5 meV); $q^{3-}_{2,\rm inter}$, ($\approx$ 143 meV); and the last one, the quadruple electrons $q^{4-}_{\rm inter}$,($\approx$ 163 meV).

From these two subpanels of the Fig. 2, the 14 mechanisms of the total 18 resonance mechanisms can be identified in the tunneling current as peaks and shoulders when the occupation number of the electron in the second QD varies from 0.5 to 1.0. The presence of shoulders results mainly from the fact that the corresponding resonance mechanism has a lower probability than the neighbouring peaks. In the last subpanel of Fig. 2 (Fig. 2(j)), the first peak corresponds precisely to the shoulder in the subpanel of $n_{2e,\sigma} = 0.5$ (Fig. 2(e)). This can be attributed to the fact that the increase of $n_{2e,\sigma}$ makes the probability for the single extra-electron attached biexciton (3e+2h complexes) $[X^2]^{(-)}_{\rm inter}$ resonance mechanism dominate over the other two neighbouring resonance mechanisms, the inter-negative-trion $X^{-}_{\rm inter}$ and the intra-negative-trion $X^{-}_{\rm intra}$ (see Fig. 2(e)). The other three sharp peaks in Fig. 2(j) are the consequences of the boosting of the corresponding tiny peaks in Fig. 2(e).

In Figs. 1 and 2, there exist common phenomena that both the plateaus for the electron occupation number and the tunneling current peaks in the main QD experience shift to the higher gate voltage (eV_g) side. The first prominent plateau ($n_{2e,\sigma} = 0.1$) in Fig. 1 becomes diminishing with the growing of $n_{2e,\sigma}$ and disappears when $n_{2e,\sigma}$ reaches unity. The peaks in the lower gate voltage side are suppressed while the peaks in the higher voltage side begin to dominate. This can be interpreted as the effect of the Coulomb interactions' competition between the charged carriers in the intra-dot and inter-dot mechanisms on the transport properties of the main QD. That is to say, the occupation number $n_{2e,\sigma}$ in the second QD influences the tunneling through adjusting the probabilities of the different resonance mechanisms. When the

occupation number is small, the tunneling current is determined by the Coulomb interaction processes in the main QD, with the increment of the occupation number $n_{2e,\sigma}$, the inter-dot Coulomb interactions begin to take effect, leading to the generation of the rich structures of the tunneling current.

As a matter of fact, almost all resonance mechanisms can be resolved by decreasing the tunneling rate $\Gamma_{L(R)}$. Figure 3 shows the occupation number $N_{e,\sigma}$ in the main QD, when the tunneling rate $\Gamma_L = \Gamma_R$ has been set to 0.1. The original main plateaus of the occupation number in Fig. 1 begin to split in Fig. 3, and more tiny plateaus emerge. The peaks in tunneling current in Fig. 4 become sharper and the linewidths of the peaks become narrower due to the lessening of the flow in/out of electrons in the main QD and the increase of the lifespan for the electron's dwelling in the main QD. Compared to the counterpart subpanel of Fig. 2 for the case of $n_{2e,\sigma} = 0.5$, the amplitude of the tunneling current in Fig. 4 becomes diminished and the original shoulders in Fig. 2 begin to form clear-cut satellite peaks due to reduction of the broadening of the peaks' width. The resonance mechanisms of the 12 peaks in Fig. 3 correspond precisely to the mechanisms for the peaks as well as shoulders in Fig. 2.

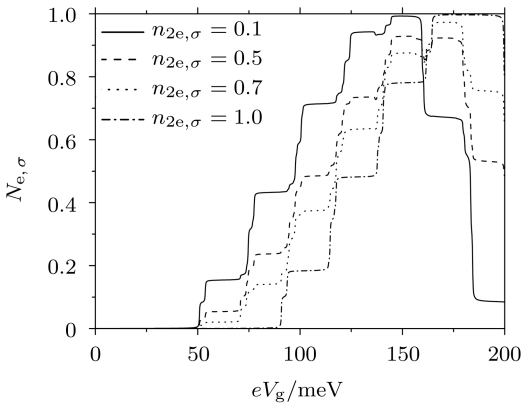


Fig. 3. Same as Fig. 1, except that the tunneling rate $\Gamma_{L(R)}$ has been set to be 0.1, resolving almost all 18 resonance mechanisms discussed in the text.

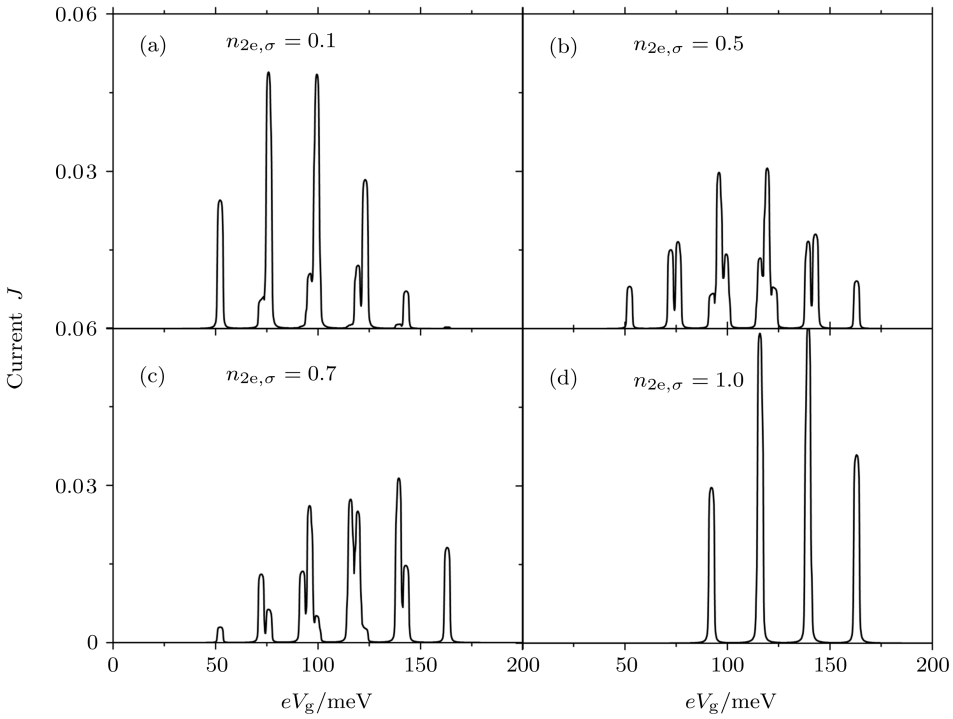


Fig. 4. The plot of the tunneling current in the main quantum dot using the same parameters as those in Fig. 3.

The electron occupation number and the tunneling current in the main QD at the finite temperature $k_BT = 2$ meV have also been studied, which are shown in Figs. 5 and 6 respectively. The broadening effect from the finite temperature is clearly seen in Fig. 5, where the sharp plateaus are blurred.

For the tunneling current, we only give the cases of $n_{2e,\sigma} = 0.1, 0.5, 0.7, 1.0$. The tunneling current bears the similar trend to those in Fig. 1, namely, the inter-dot interaction mechanisms dominate the tunneling processes with the increase of the electron occupation number in the second QD. By comparing the tunneling current peaks for the case of $n_{2e,\sigma} = 0.5$ in Fig. 6(b) to the counterpart in Fig. 2(e), it is found that the satellite peaks in Fig. 2(e) have merged together forming six main peaks in Fig. 6(b) due to the thermal broadening. Among these six main peaks, some of the peaks can be regarded as the linear mixing of two or three peaks. For example, the second peak in Fig. 6(b) is the admixture of the inter-biexciton $[X^2]_{\rm inter}$ and intra-exciton $[X]_{\rm intra}$ in Fig. 2(e); the third peaks are the admixture of the inter-negative-trion $X^-_{\rm inter}$, with the two satellite peaks, inter-negative trion $X^-_{\rm inter}$, and intra-negative-trion $X^-_{\rm intra}$, in Fig. 2(e).

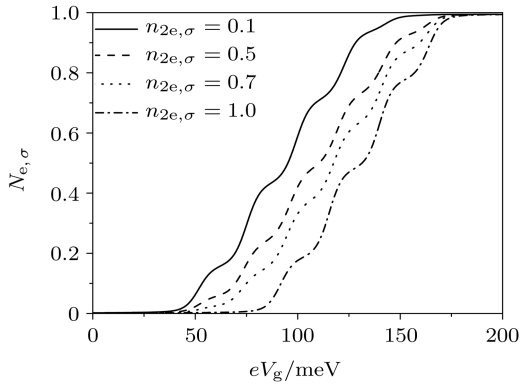


Fig. 5. The finite temperature counterpart plot of the Fig. 1 at $k_BT = 2$ meV.

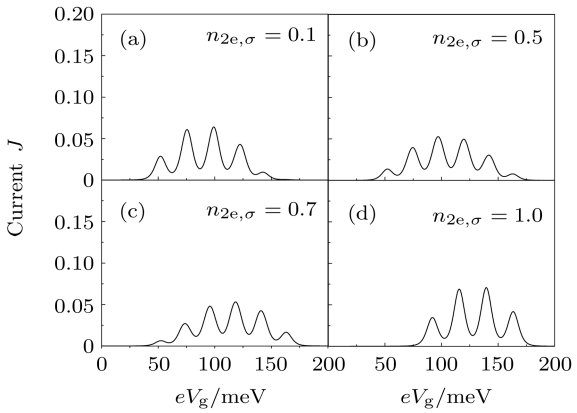


Fig. 6. The tunneling current in the main QD plotted as a function of the gate voltage eV_g for different electron occupation numbers in the second QD, where the same parameters as those in Fig. 5 are used.

The actual position of a certain main peak in Fig. 6(b) is determined by the resonance energies as well as the corresponding probability. For example, the second peak's position in Fig. 6(b) is located around the half way of the two participating peaks in Fig. 2(e), which have the almost equal resonance peaks' ampltudes (viz. equal probabilities). While the position for the third peak in Fig. 6(b) is mainly determined by the middle peaks in Fig. 2(e), which has the highest peaks (viz. the largest probability).

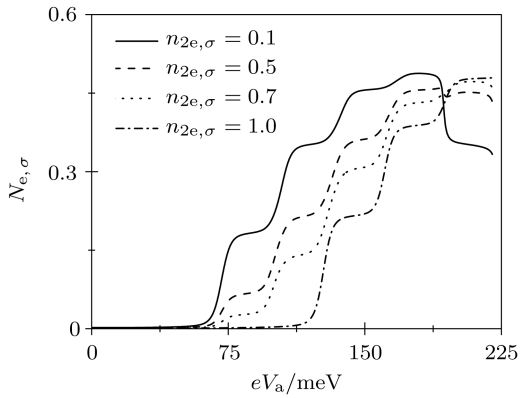


Fig. 7. The occupation number of electrons in the main QD versus the bias potential eV_a for different occupation numbers of electron in the second QD at finite temperature; the gate voltage eV_g has been set to vanishing, and the other parameters are the same as those in Fig. 5.

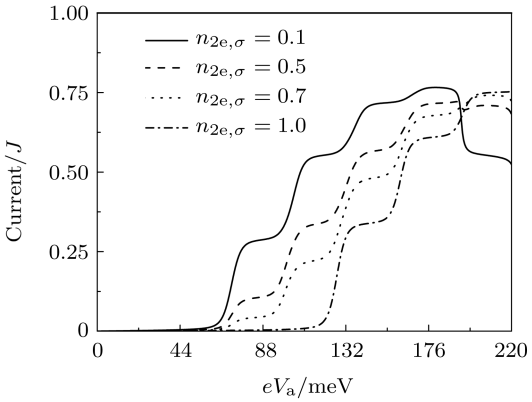


Fig. 8. The plot of the tunneling current versus the bias potential eV_a, where the same parameters are used as those in Fig. 7.

The electron occupation number and tunneling current in the main QD have also been calculated as the functions of the source-drain bias voltage V_a. The electron occupation number in the main QD reaches the saturation state at different biases with the different electron occupation numbers in the second QD (shown in Fig. 7). The larger the electron occupation number attains in the second QD, the higher the source-drain bias is required to make the electron occupation number in the main QD culminate. The tunneling current versus the source-drain bias is plotted

in Fig. 8, where Coulomb staircases can be distinctly identified.

It can be seen from the figure that the introduction of the second QD makes the attraction-repulsion resonance complexes flourish, leading to the gain of the tunneling channels for the electron–hole complexes to pass through. This effect can be seen in the cases of $n_{2e,\sigma} = 0.5, 0.7$ in Fig. 8, where the common actions from both the inter and intra electron–hole complexes induced resonance mechanisms render the rich structures of the Coulomb staircases.[31] For the extreme cases where $n_{2e,\sigma} = 1.0$, the first plateau for both the electron occupation number and tunneling current in the main QD are shifted toward the larger bias voltage V_a, and some plateaus completely disappear. All these mean that the *inter* resonance mechanisms will dominate the tunneling processes with the increase of the electron occupation number introduced in the second QD. In technical viewpoint, one can use this effect to switch on/off the electron tunneling in the main QD for a particular plateau by modulating the electron occupation number in the second QD.

4. Concluding remark

In summary, we have investigated the quantum tunneling processes from the Coulomb-coupled QDs embedded in the n–n junction. Using the Keldysh formalism, the analytical expression for the tunneling current through the main QD has been obtained. Eighteen resonance mechanisms in the tunneling current have been found analytically and interpreted term by term, making it clear that the introduction of the second QD not only increases the resonance mechanisms in the system but also modifies the probability for a certain resonance. Further numerical analysis shows that the electron occupation number in the second QD influences significantly both the occupation number plateaus and tunneling current peaks in the main QD. The effect of Coulomb interactions among the charged carriers in the main and the second QDs on the transport processes can be classified into two classes, intra-resonance mechanisms in the main QD and inter-resonance mechanisms between the two Coulomb-coupled QDs. With the increase of electron occupation number in the second QD, the coexistence of the intra- and inter-resonance mechanisms appear both in the tunneling current and the occupation number plateaus. The inter-resonance mechanisms dominate the tunneling current when the electron occupation number in the second QD reaches the maximum. Some of the fine resonance structures found in the tunneling current can provide a clue for the applications of the Coulomb interactions among the carriers to the quantum information processing.[13,23,25,26,28,29]

References

[1] Jacak L, Hawrylak P and Wojs A 1998 *Quantum Dots* (Berlin: Springer-Verlag)
[2] Petroff P M, Lorke A and Imamoglu A 2001 *Phys. Today* **54** 46
[3] Bhattacharya P, Ghosh S and Stiff-Roberts A D 2007 *Proceedings of the IEEE* **95** 1723
[4] Loss D and DiVincenzo D P 1998 *Phys. Rev.* A **57** 120
[5] Ouyang M and Awschalom D D 2003 *Science* **301** 1074
[6] Liu K, Ding H L, Zhang X G, Yu L W, Huang X F and Chen K G 2008 *Acta Phys. Sin.* **57** 7052 (in Chinese)
[7] Xu T N, Wu H Z and Si J X 2008 *Acta Phys. Sin.* **57** 2574 (in Chinese)
[8] Huang S S, Niu Z C, Zhan F, Ni H Q, Zhao H, Wu D H and Sun Z 2008 *Chin. Phys.* B **17** 1674
[9] Goldhaber-Gordon D, Montemerlo M S, Love J C, Opiteck G J and Ellenbogen J 1997 *Proceedings of the IEEE* **85** 521
[10] Kuo David M T and Chang Y C 2005 *Phys. Rev.* B **72** 085334
[11] Findels F, Baier M, Duijs E, Beham E, Bichler M, Zrenner A, Hohenester U and Molinari E 2001 Kramer E B (ed.) *Adv. in Solid State Phys.* **41** 63
[12] Chen G L, Kuo David M T, Lai W T and Li P W 2007 *Nanotechnology* **18** 475402
[13] Danckwerts J, Ahn K J, Förstner J and Knorr A 2006 *Phys. Rev.* B **73** 165318
[14] Fält S, Atatüre M, Türeci H E, Zhao Y, Badolato A and Imamoglu A 2008 *Phys. Rev. Lett.* **100** 106401
[15] Hawrylak P, Sheng W and Cheng S J 2004 *Acta Phys. Pol.* A **106** 403
[16] Cheng S J, Sheng W and Hawrylak P 2003 *Phys. Rev.* B **68** 235330
[17] Ediger M, Bester G, Gerardot B D, Badolato A, Petroff P M, Karrai K, Zunger A and Warburton R J 2007 *Phys. Rev. Lett.* **98** 036808
[18] Kuo David M T and Chang Y C 2007 *Phys. Rev. Lett.* **99** 086803
[19] Chang Y C and Kuo David M T 2008 *Phys. Rev.* B **77** 245412
[20] Landin L, Miller M S, Pistol M E, Pryor C E and Samuelson L 1998 *Science* **280** 262
[21] Chu W D, Duan S Q and Zhu J L 2007 *Appl. Phys. Lett.* **90** 222102
[22] Shabaev A, Efros Al L, Gammon D and Merkulov I A 2003 *Phys. Rev.* B **68** 201305(R)

[23] Chen P, Piermarocchi C, Sham L J, Gammon D and Steel D G 2004 *Phys. Rev.* B **69** 075320
[24] Szafran B, Barczyk E, Peeters F M and Bednarek S 2008 *Phys. Rev.* B **77** 115441
[25] Michler P, Kiraz A, Becher C, Schoenfeld W V, Petroff P M, Zhang L, Hu E and Imamoglu A 2000 *Science* **290** 2282
[26] Santori C, Pelton M, Solomon G, Dale Y and Yamamoto Y 2001 *Phys. Rev. Lett.* **86** 1502
[27] Yang X, Xiang S H and Song K H 2008 *Chin. Phys.* B **17** 435
[28] Li X Q and Yan Y J 2002 *Appl. Phys. Lett.* **81** 168
[29] Nazir A, Lovett B W and Briggs G A D 2004 *Phys. Rev.* A **70** 052301
[30] Wen Y B and Yan W X 2008 *Phys. Rev.* A **77** 052332
[31] van der Wiel W G, De Franceschi S, Elzerman J M, Fujisawa T, Tarucha S and Kouwenhoven L P 2002 *Rev. Mod. Phys.* **75** 1
[32] Jeong H, Chang A M and Melloch M R 2001 *Science* **293** 2221
[33] Chen M L and Wang S J 2007 *Chin. Phys.* **16** 2101
[34] Chen M L and Wang S J 2007 *Chin. Phys.* **16** 2096
[35] Sun K W and Xiong S J 2006 *Chin. Phys.* **15** 828
[36] Yan C H, Wu S Q, Huang R and Sun W L 2008 *Chin. Phys.* B **17** 296
[37] Bai A H, Wu S Q and Hou T 2008 *Chin. Phys. Lett.* **25** 3028
[38] Yang F B, Wu S Q and Sun W L 2007 *Chin. Phys. Lett.* **24** 2056
[39] Lü R and Liu Z R 2007 *Chin. Phys. Lett.* **24** 195
[40] Kuo David M T and Chang Y C 2004 *Phys. Rev.* B **69** 041306(R)
[41] Heitz R, Born H, Guffarth F, Stier O, Schliwa A, Hoffmann A and Bimberg D 2001 *Phys. Rev.* B **64** 241305(R)
[42] Jauho A P, Wingreen N S and Meir Y 1994 *Phys. Rev.* B **50** 5528
[43] Meir Y, Wingreen N S and Lee P A 1993 *Phys. Rev. Lett.* **70** 2601